Pharmaceutical Sciences, 2024, 30(4), 456-468
doi:10.34172/PS.2024.20
https://ps.tbzmed.ac.ir/

Research Article

A Lead Optimization of TOPK Inhibitors Using Complementary Computational and Synthetic Approaches

Manar Al-Sarhan[1], Lara I. Fakhouri[1*], Nizar A. Al-Shar'i[1,2*], Tamam El-Elimat[1], Aref Zayed[1]

[1]*Department of Medicinal Chemistry and Pharmacognosy, Faculty of Pharmacy, Jordan University of Science and Technology, P.O. Box 3030, Irbid, Jordan.*
[2]*Department of Pharmaceutical Sciences, College of Pharmacy, Qatar University, P.O. Box 2713, Doha, Qatar.*

Article Info

Article History:
Received: 23 Feb 2024
Accepted: 2 Jul 2024
ePublished: 23 Jul 2024

Keywords:
-Molecular docking
-N^2,N^7-dibenzyl-9-oxo-9*H*-fluorene-2,7-disulfonamide
-TOPK

Abstract

Background: T-LAK cell-originated protein kinase (TOPK), a member of the MEK3/6-related mitogen-activated protein kinase kinase (MAPKK) family, is highly overexpressed in various cancers. This overexpression is linked to the mitotic phase of the cell cycle, highlighting its potential as a prognostic marker and therapeutic target. Unlike many other cancer targets, TOPK exhibits limited expression or is even absent in non-proliferative tissues. Therefore, TOPK inhibitors hold promise for developing anticancer agents with high selectivity and specificity for cancer cells, potentially leading to fewer side effects compared to conventional therapies. This study builds on our previous success in identifying TOPK inhibitors and aims to optimize them for improved potency

Methods: An integrated approach combining computational modeling and organic synthesis was employed. Ninety-two analogs of the lead compound (N^2,N^7-dibenzyl-9-oxo-9H-fluorene-2,7-disulfonamide) were designed virtually and assessed for binding affinity to TOPK using docking simulations. Eight top-scoring analogs were synthesized and their inhibitory activity against TOPK was evaluated *in vitro*.

Results: The *in-silico* analysis identified eight promising analogs. However, the most active synthesized analog (compound 10) exhibited moderate inhibitory activity (IC_{50} = 86 µM) compared to the lead compound (IC_{50} = 54 µM).

Conclusion: While the computational approach identified potential candidates, further optimization of the synthetic analogs is necessary to achieve superior TOPK inhibitory activity. This study highlights the value of a combined computational and synthetic strategy for TOPK inhibitor development. TOPK inhibitory activity. This study highlights the value of a combined computational and synthetic strategy for TOPK inhibitor development.

Introduction

Cancer is characterized by abnormal cell proliferation resulting from genetic changes that impact the cell cycle.[1,2] Globally, cancer remains the second leading cause of death. According to GLOBOCAN estimates on cancer incidence and mortality rates, the number of new cancer cases is projected to rise to 30 million in 2024, up from 19.3 million in 2020.[3] Despite an anticipated decline in the number of deaths, the need for exploiting and targeting new pathways is of utmost importance, primarily due to the continuous development of resistance.[4] Small molecule kinase inhibitors are a novel targeted therapy for various cancers. It is a unique field in the development of anti-cancer treatments with more selectivity and effectiveness against cancer cells while minimizing harm to normal cells.[5,6]

Targeting protein kinases, that regulate the function of other proteins through phosphorylation, has emerged as a significant field in treating various diseases including hypertension, Parkinson's disease, inflammatory and autoimmune diseases, and cancer.[7] Following the approval of Gleevec (imatinib), a selective inhibitor of the BCR-ABL tyrosine kinase specifically designed for the treatment of chronic myeloid leukemia, the FDA has subsequently approved 72 therapeutic agents.[8] This underscores the significance of small molecule kinase inhibition as a pivotal approach in treating various diseases, particularly cancer.[9]

TOPK (T-lymphokine-activated killer-cell-originated protein kinase) has recently emerged as a promising target for cancer-specific drugs. It is a serine-threonine kinase with 322 amino acids and plays a key role in cell division, particularly cytokinesis.[10-12] TOPK is overexpressed in many tumor tissues, and its upregulation is significantly correlated with the malignancy, poor prognosis and drug resistance of these tumors.[13] The high expression

*Corresponding Authors: Lara I. Fakhouri, E-mail: lialfakhori@just.edu.jo, Nizar A. Al-Shar'i, E-mail: nashari@just.edu.jo

of TOPK in proliferative tissues, coupled with lack of expression in non-proliferative tissues, makes TOPK a compelling target for achieving maximum selectivity and minimal side effects compared to other prospective kinase inhibitors.[10,14,15]

The only available crystal structure of TOPK was solved by *Dong et al.* who successfully crystalized a double mutant TOPK dimer (PDB accession code is 5J0A).[16] The N-lobe of the enzyme dimer is distorted, and in a previous work of our group a 3D homology model of the enzyme was constructed (Figure 1A) and utilized to identify novel TOPK inhibitors (Figure 1B) using different computational methods.[17]

This study is a continuation of our previous work aiming to design new TOPK inhibitors with improved inhibitory activities. Although less active than the other identified hits, compounds **1** and **2** were chosen as leads for optimization due to their synthetic feasibility and readily available precursors. A set of analogs were proposed based on their chemical structure, and their binding modes and estimated binding energies were calculated using different computational protocols available in Discovery Studio (DS) 2020 from Biovia® Software Inc.[18] The best scoring analogs were then synthesized, fully characterized, and their biological activities were evaluated using *in vitro* biochemical assays.

Methods

Materials

Computational materials

All proposed analogs were sketched using ChemDraw Professional 16 version (16.0.0.82). All *in silico* modeling steps, including compounds preparation, molecular docking, *in situ* ligand minimization, and binding energy calculations were performed using Discovery Studio.

Experimental materials

All experiments were conducted under a dry nitrogen atmosphere using pre-dried glassware. Commercially available solvents and reagents were used directly without further purification. Merck silica gel 60 F254 plates (0.25 mm thickness) were used for TLC. Visualization was achieved with a 254 nm UV lamp.

Products were purified by normal-phase chromatography using a Buchi™ system (Switzerland). Flash columns (Salicycle® silica gel, particle size: 40-63 µm, mesh: 230-400) were purchased from Buchi Laboratory Equipment. The purification process employed a flow rate of 4.7 mL/min with detection at λmax = 366 nm. The purity of the synthesized compounds was further evaluated using high-performance liquid chromatography (HPLC). A gradient mobile phase system was employed, consisting of a phosphate buffer (pH 7) and acetonitrile. The separation was achieved on a Kinetex XB-C18 column (30 x 2.1 mm, 2.6 microns) from Phenomenex.

^{1}H NMR spectra were recorded on a Bruker 400 MHz spectrometer using the specified solvent. The experiments were run at 17 °C, except for DMSO-d6 (run at 25 °C). Chemical shifts are reported in δ units (ppm) relative to tetramethylsilane (TMS) with reference to solvent peaks (chloroform: 7.26 ppm, methanol: 3.31 ppm, acetone: 2.05 ppm, dimethyl sulfoxide: 2.50 ppm). Similar referencing was used for ^{13}C NMR spectra (chloroform: 77 ppm, methanol: 49 ppm, acetone: 29.8 ppm, dimethyl sulfoxide:

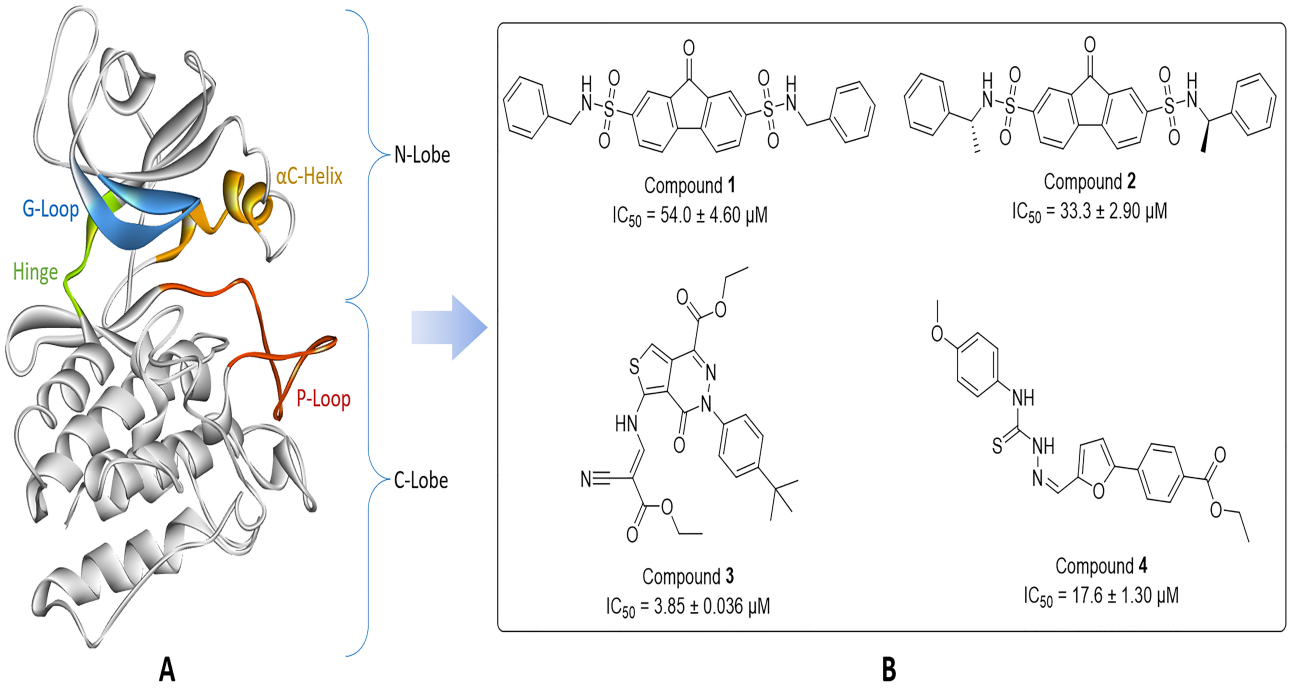

Figure 1. A. The 3D homology model of TOPK with its subdomains and loops being highlighted. B. The chemical structure of the previously identified TOPK inhibitors.

39.5 ppm) with ^{1}H decoupling. High-Resolution Mass Spectrometry (HRMS) Data were obtained using an Agilent liquid chromatography/mass spectrometry (LC/MS) system.

Computational Methods

Design of new potential TOPK inhibitors

The design of new analogues was guided by thorough analysis of the binding interactions and binding modes of the lead compounds **1** and **2** , particularly focusing on varying the chemical space of the nitrogen substituents. This approach aimed to explore a broader range of potential interactions with the TOPK binding pocket.

Preparation of proposed analogs

All proposed analogs were prepared using the *Prepare Ligands* protocol to generate isomers, tautomers, and ionization states of the analogs. The parameters for generate isomer was set to false, and that for generate tautomer was set to canonical tautomer.

Molecular docking

The previously refined 3D homology model of the TOPK enzyme was used as a structural model for docking study. The prepared analogs were docked into the ATP-binding site of the enzyme (previously defined) using the *Dock Ligands (CDOCKER)* protocol in DS with default parameters.[19]

In situ ligand minimization, and calculation of binding energy

The generated docked poses were *in situ* minimized within the binding site of the enzyme using the *In Situ Ligand Minimization* protocol using default parameters except for hydrogen flexibility which was set to true. Then, the free binding energies of all docked poses were calculated using the *Calculate Binding Energies* protocol, where solvents effects were accounted for using the molecular Mechanics Poisson Boltzmann with non-polar surface area (MM-PBSA) implicit solvent model.[17]

Analyze ligand pose

All docked poses of the proposed compounds were analyzed using the *Analyze Ligand Poses* protocol which calculates and statistically analyze non-bonded interactions (such as hydrogen bonds, electrostatics, hydrophobic, and others) between a target and ligand poses. All parameters were kept at their default values. The docked poses of the four previously identified hit compounds were also included in the calculation to aid in the analysis and selection of potential inhibitors from the proposed set of analogs.

Synthesis

The best scoring selected analogs were synthesized following the general procedure outlined in Figure 2. In this scheme, 9-fluorenone was reacted with chlorosulfonic acid to generate the meta-dichlorosulfonated intermediate **5.**[13] Subsequently, this intermediate was coupled with the substituted amine to give the corresponding analogs **1, 6-13**.[20]

Biological evaluation

The *in vitro* biological activity of the synthesized compounds was assessed by the TOPK enzyme assay performed by the Reaction Biology Corp. (Malvern, PA, USA). Compounds were dissolved in DMSO to a final stock concentration of 10 mM. TOPK inhibition was assessed at 10 different concentrations with 3-fold serial dilution starting at 50 µM and descending to 2.54 nM. The percentage of inhibition was calculated in duplicate, and the IC_{50} was determined using PRISM. Staurosporine, which is used as the control compound, underwent a 4-fold serial dilution starting at 20 µM and was tested in 10-dose IC_{50} mode. Reactions were conducted with a 10 µM ATP. Two controls were employed in the IC_{50} determination of which are the MAX (DMSO, 100% activity) and MIN (25 mM EDTA, final concentration, MIN activity).[21]

The *in vitro* assay was performed as follows; TOPK/

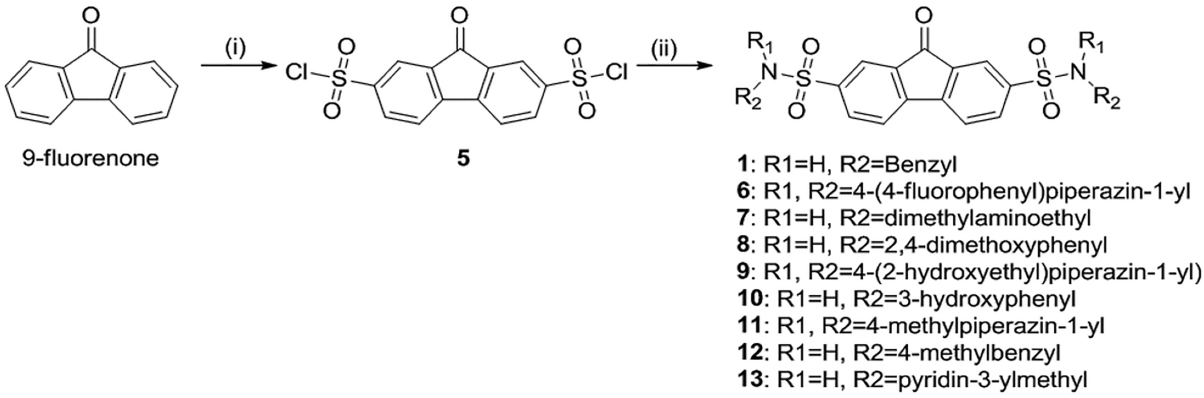

Figure 2. General synthetic scheme of N^2,N^7-disubstituted-9-oxo-9H-fluorene-2,7-disulfonamide Analogs. Reagents and conditions: (i) $ClSO_3H$, 150 °C, 5 days. (ii) R^1R^2NH, Et_3N, DCM, r.t, 24 h.

substrate (Myelin Basic Protein) pair along with required cofactors were prepared in reaction buffer; 20 mM Hepes pH 7.5, 10 mM $MgCl_2$, 1 mM EGTA, 0.01% Brij35, 0.02 mg/ml BSA, 0.1 mM Na_3VO_4, 2 mM DTT, and 1% DMSO. Compounds were delivered into the reaction, followed ~20 min later by the addition of a mixture of ATP (Sigma) and 33P ATP (PerkinElmer) to a final concentration of 10 µM. Reactions were carried out at 25°C for 120 min, followed by spotting of the reactions onto P81 ion exchange filter paper (Whatman). Unbound phosphate was removed by extensive washing of filters in 0.75% phosphoric acid. After subtracting the background derived from control reactions containing inactive enzyme, kinase activity data were expressed as the percent remaining kinase activity in test samples compared to vehicle (dimethyl sulfoxide) reactions.[21]

Results and Discussion

TOPK is highly expressed and activated in rapidly dividing cells. This recognition of TOPK's role in cancer cell proliferation has driven researchers to discover and develop inhibitors targeting this promising therapeutic target.[22-24] OTS514 (IC_{50}=3 nM) was identified via high throughput screening. Extensive structural optimization of OTS514 led to OTS964, which offered improved bioavailability despite slightly lower potency (IC_{50} = 28 nM).[25,26] However, both OTS514 and OTS964, while effective in inhibiting tumor growth in both cell culture and animal models, caused hematopoietic toxicity (Figure 3).[25] Despite the identification of over 20 additional potent TOPK inhibitors, none have surpassed the efficacy and safety profile of the phenyl phenanthridinone derivatives, OTS514 and OTS964. Therefore, the search for novel chemical scaffolds to discover more effective and well-tolerated TOPK inhibitors remains ongoing.

The TOPK homology model, constructed by our research team, has demonstrated success in the identification of promising hits.[17] This success has prompted us to employ this model in the optimization of these hits, aiming to elucidate the structure-activity relationship of the diverse chemical scaffolds and improve their potency.

While not the most potent hits, the selection of the fluorenone compounds **1** and **2** in the initial round of optimization is based on several key considerations. The symmetrical nature of the 2,7-disulfonylamide fluorenone facilitates the feasibility of chemical synthesis. Moreover, the flat configuration of the fluorenone ring, combined with a high aromatic ring count and low percentage of sp3 carbons, corresponds with recognized determinants of kinase inhibitors.[27] It is worth mentioning that other biomolecules such as Telomerase[28] and urea transporters[29] are among established targets of symmetrical 2,7-disubstituted fluorenone highlighting the diverse pharmacological activity of these compounds.

In this stage of optimizing potential TOPK inhibitors, the 9H-flourenone flat ring along with the sulfonamide groups were conserved and modification focused on diversifying the chemical space of the *N*-substituents to include primarily alicyclic, aromatic, and heteroaromatic rings. Our proposal includes a total of 92 compounds, which were sketched using ChemDraw and subsequently exported to Discovery Studio (DS) for further computational investigation and analysis.

Computational approach

Design and preparation of proposed analogs

A new set of 92 analogs were proposed as new potential TOPK inhibitors based on the chemical structure of previously identified hits. Before docking the proposed compounds into the active site of the TOPK homology model, the compounds were prepared using the *Prepare Ligands* protocol in DS. This protocol generates the most stable tautomer(s) (canonical tautomer), ionization states of ionizable functional groups of the compounds at a pH range of 6.5 to 8.5, and coordinates for 3D structures. The 92 proposed analogs along with the two leads produced 118 prepared compounds.

Molecular docking

The *Dock Ligands (CDOCKER)* protocol was used in docking the prepared compounds into the active site of the

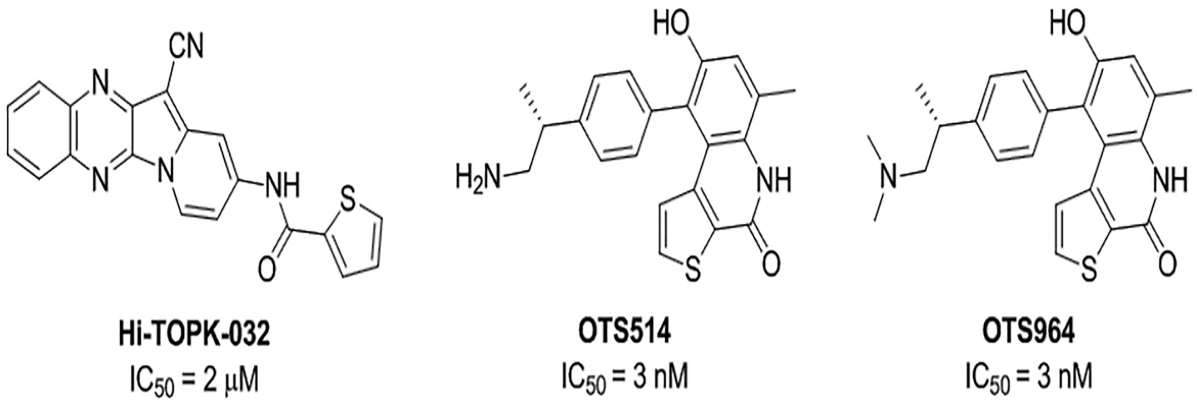

Figure 3. Structures of TOPK inhibitors

TOPK homology model. CDOCKER uses a CHARMm-based molecular dynamics (MD) and simulated annealing algorithm to generate random ligand conformations poses (conformations) followed by a final minimization step of the selected poses in the binding site of the rigid target. Further, it uses a force-field scoring function to score and rank the docked poses.[30] The calculated CDOCKER scores are the CDOCKER Energy (interaction energy plus ligand strain) and the CDOCKER interaction energy, which indicate ligand binding affinity. The lower (more negative) the values the better the binding affinity.

The 118 prepared hits were docked into the ATP-binding site of the TOPK homology model to generate 1180 poses with -CDOCKER energy ranging from -29.5891 (unfavorable) to 67.7221 (favorable) kcal/mol and -CDOCKER interaction energy ranging from 35.6737 to 92.5352 kcal/mol.

In situ ligand minimization and calculation of binding energy

In order to obtain a more robust estimation of ligands' binding energies, the *Calculate Binding Energies* protocol was used. However, prior to that, all docked poses were minimized within the TOPK active site using the *In Situ Ligand Minimization* protocol. This protocol is a CHARMm-based protocol of minimization that minimizes the energy of docked poses within the active sites of the target. This protocol calculates and then scores the results as negative values of In-Situ Start Energy and In-Situ Final Energy in kcal/mol before and after minimization respectively.

Following the in situ minimization of the 1180 poses, their binding energies were calculated using the *Calculate Binding Energies* protocol which uses CHARMm energies and an implicit solvent model, to account for solvent effects, for binding energy calculations. The favorable interaction between the target and a ligand must give a negative value of binding energy. Therefore, the most negative binding energy values correspond to the most favorable interactions. In this study, the Poisson Boltzmann with non-polar surface area (PBSA) implicit solvent model was used.[31,32] The binding energy values of the best scoring pose (most negative value) for each of the 92 docked compounds ranged from -42.47 (favorable) to 21.52 (unfavorable) kcal/mol. It is worth mentioning that the calculated binding energy values are more accurate than those obtained from docking scores since the solvent effects are accounted for in the former.

Analysis of the docked poses

All 1180 docked poses in addition to those of the two leads were analyzed using the *Analyze Ligand Poses* protocol to calculate the nonbonded interactions between the docked poses and amino acids of the TOPK binding site (Figure 4). By analyzing the amino acids that form hydrogen bonds with the previously identified four lead compounds and comparing them with those interacting with the 92 proposed analogs, six amino acids (Lys46, Ser104, Lys151, Ser153, Asp168, and Asp238) were revealed as the ones that form the highest number of hydrogen bonds with the docked compounds. Similarly, the hydrophobic interactions were formed mainly with (Leu20, Val28, Met97, Val156, and Cys167) (Figure 5). These findings indicate that the four previously identified lead compounds

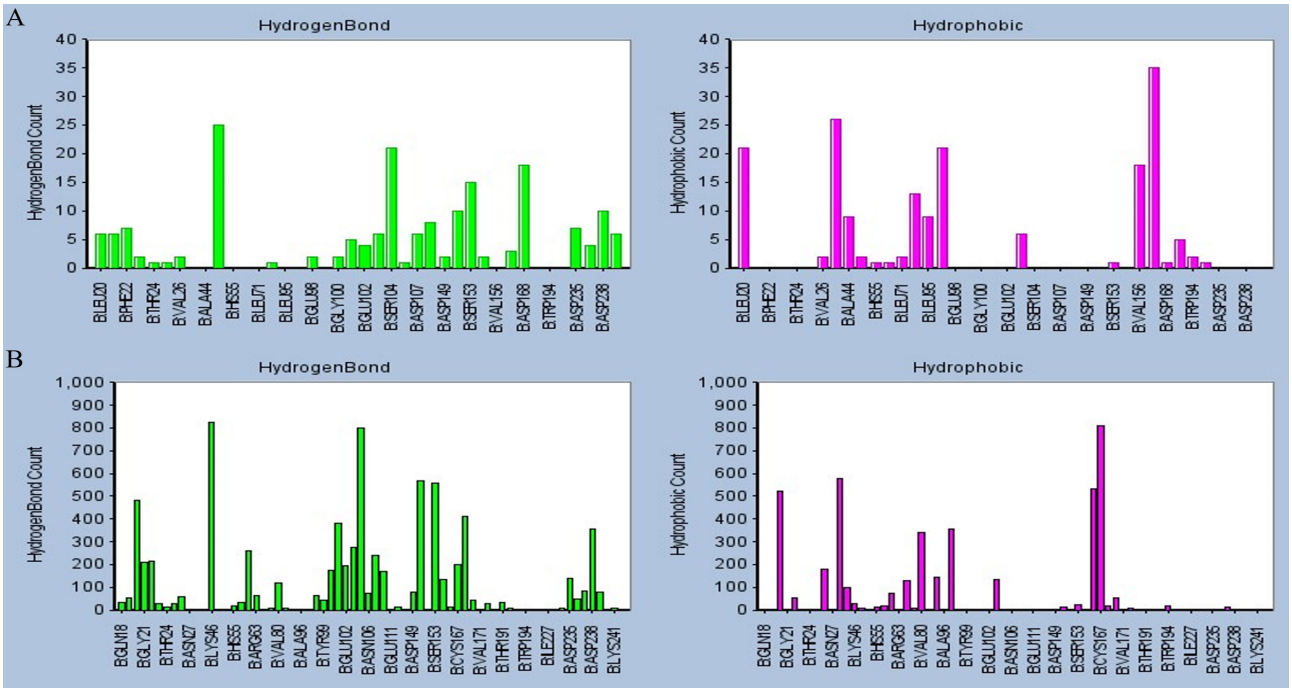

Figure 4. A. Histograms of the intermolecular interaction counts for the four previously identified lead compounds. Left: the counts of hydrogen bond interactions (in green) with active site's amino acids. Right: the counts of the hydrophobic interactions (in pink). (B): Histograms of the intermolecular interaction counts for proposed compounds. Left: the counts of hydrogen bond interactions. Right: the counts of the hydrophobic interactions.

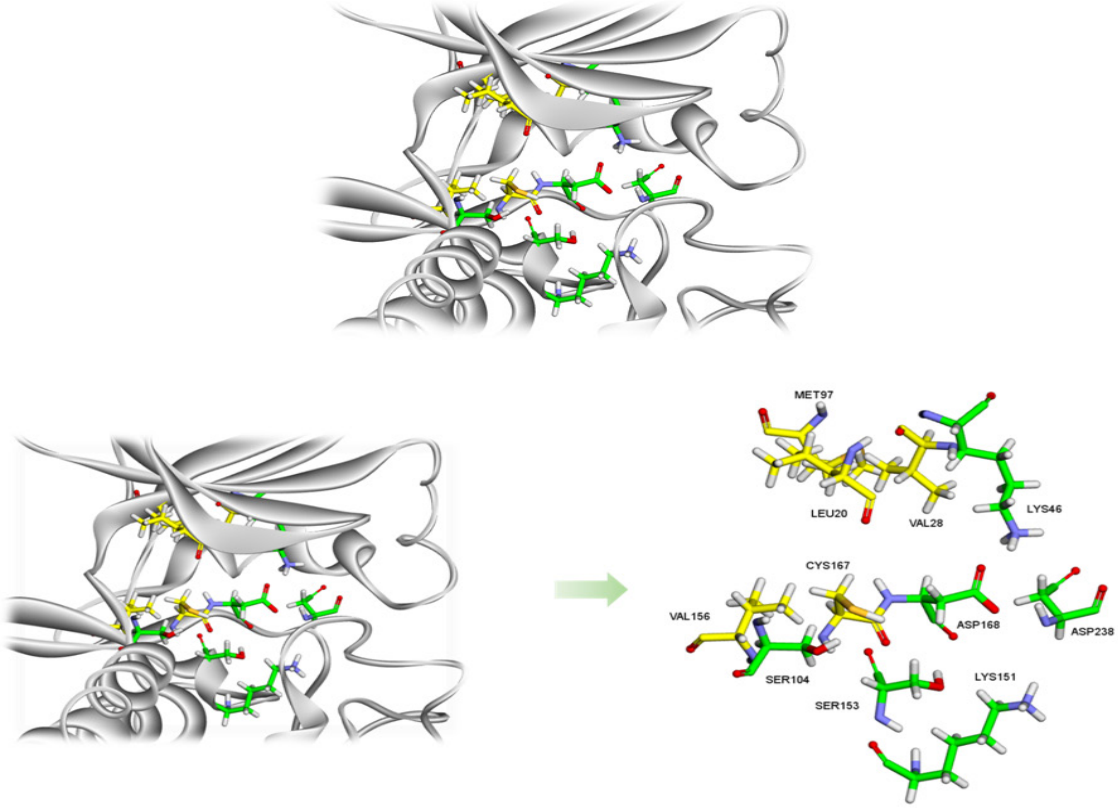

Figure 5. The amino acids in the ATP binding site that formed hydrogen bonds (green carbons) and hydrophobic interactions (yellow carbons) with the docked compounds.

and the proposed analogs occupy the same binding site in the ATP pocket and form similar interactions. Interactions with these amino acids can aid in the selection of proposed analogs that will be later synthesized.

Selection of the best scoring compounds to be synthesized

The selection of potential TOPK inhibitor among the proposed analogs followed a sequential filtration process which involved different criteria including consideration of the -CDOCKER energy and -CDOCKER interaction energy scores which retrieved 84 compounds; then compounds that showed binding energy values of less than -18 kcal/mol (analogous to that of the lead compounds) were selected, which resulted in 40 compounds. Further, consideration of the structural diversity of the retrieved compounds; visual inspection of their binding modes; and consideration of the available budget had resulted in the final selection of 8 compounds (Table 1).

Based on the chemical structure of the selected compounds, they can be classified into four groups, namely the lead-like compounds (**8**,**10**,**12**), a heteroaromatic-containing compound (**13**), piperazine-containing compounds (**6**,**9**,**11**), and an aliphatic-containing compound (**7**) (Figure 6).

Analysis of the binding modes of the selected compounds

Figure 7 shows the binding modes of the top scoring poses for representative compounds (**7** and **13**) of the selected set compared to that of the lead compound **1.**

Based on the docking results, compound **1** (the lead) occupies the ATP binding site and extends to the hydrophobic pocket behind the adenine binding region. Such that, the *N*-benzylsulfonamide part binds the hydrophobic pocket where the phenyl ring forms a pi-alkyl interaction with val169, the nitrogen forms a H-bond with Asp169, and the S=O forms another H-bond with Lys46. The central fluorenone part binds the adenine binding region and forms pi-sulfur interaction with Cys167, and two pi-alkyl interactions with Val28 and Cys167. The other *N*-benzylsulfonamide which points towards the solvent, forms H-bond between the S=O and Ser104, carbon H-bond between S=O and Ser153, and a pi-pi stacking between the phenyl ring and Phe22.

Notably, compounds **7** and **13** showed different binding orientation where they were traversing the ATP binding site. However, they were forming interactions (H-bonding and hydrophobic) with the same amino acids interacting with the lead compound, namely Val28, Lys46, Ser104, Cys167, and Asp168, (in addition to other ones) as detailed in Figure 7. These numerous polar and hydrophobic interactions are indicative of good binding affinities which imply that they might show good TOPK inhibitory activities.

Table 1. The selected compounds for synthesis with -CDOCKER energies, -CDOCKER interaction energies, and total binding energies.

No	Chemical structure	-CDE[a]	-CDIE[b]	TBE[c]	IC_{50} (μM)
1	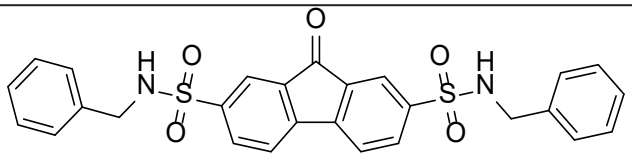	29.29	51.96	-21.48	54
2	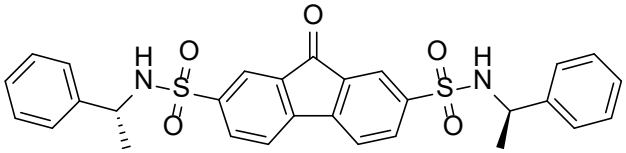	35.26	57.45	-18.70	NA
6	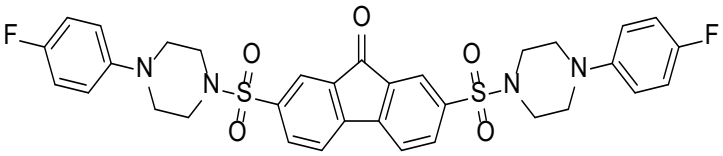	11.35	51.33	-22.23	NA
7	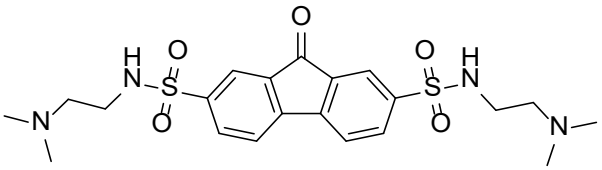	33.04	57.69	-21.04	NA
8	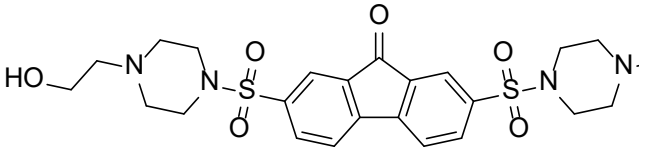	10.26	55.87	-20.26	NA
9	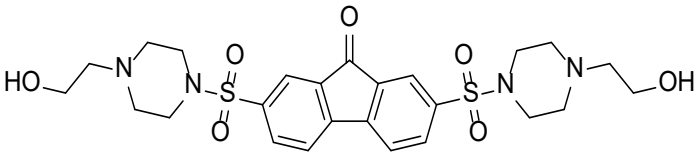	14.33	62.38	-42.46	NA
10	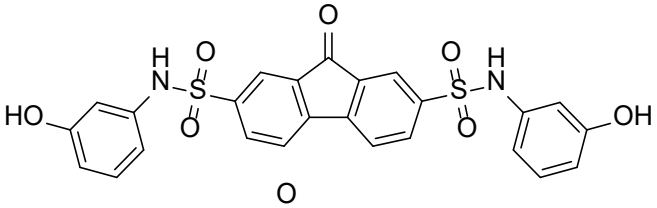	8.59	50.01	-22.05	NA
11	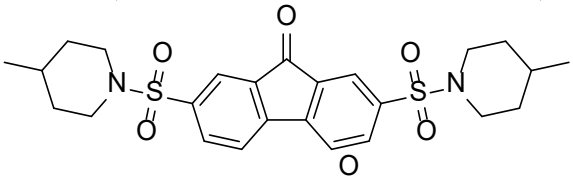	20.69	64.53	-23.70	NA
12	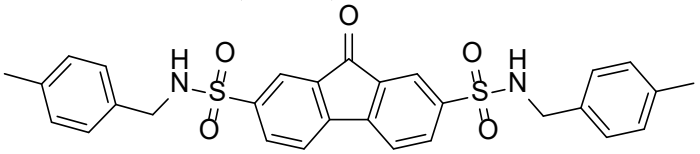	33.09	56.96	-19.88	NA
13	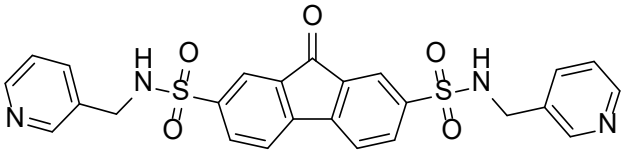	32.13	57.08	-20.29	86

[a]: The CDOCKER energy (kcal/mol).
[b]: The CDOCKER interaction energy (kcal/mol).
[c]: Binding energy (kcal/mol).

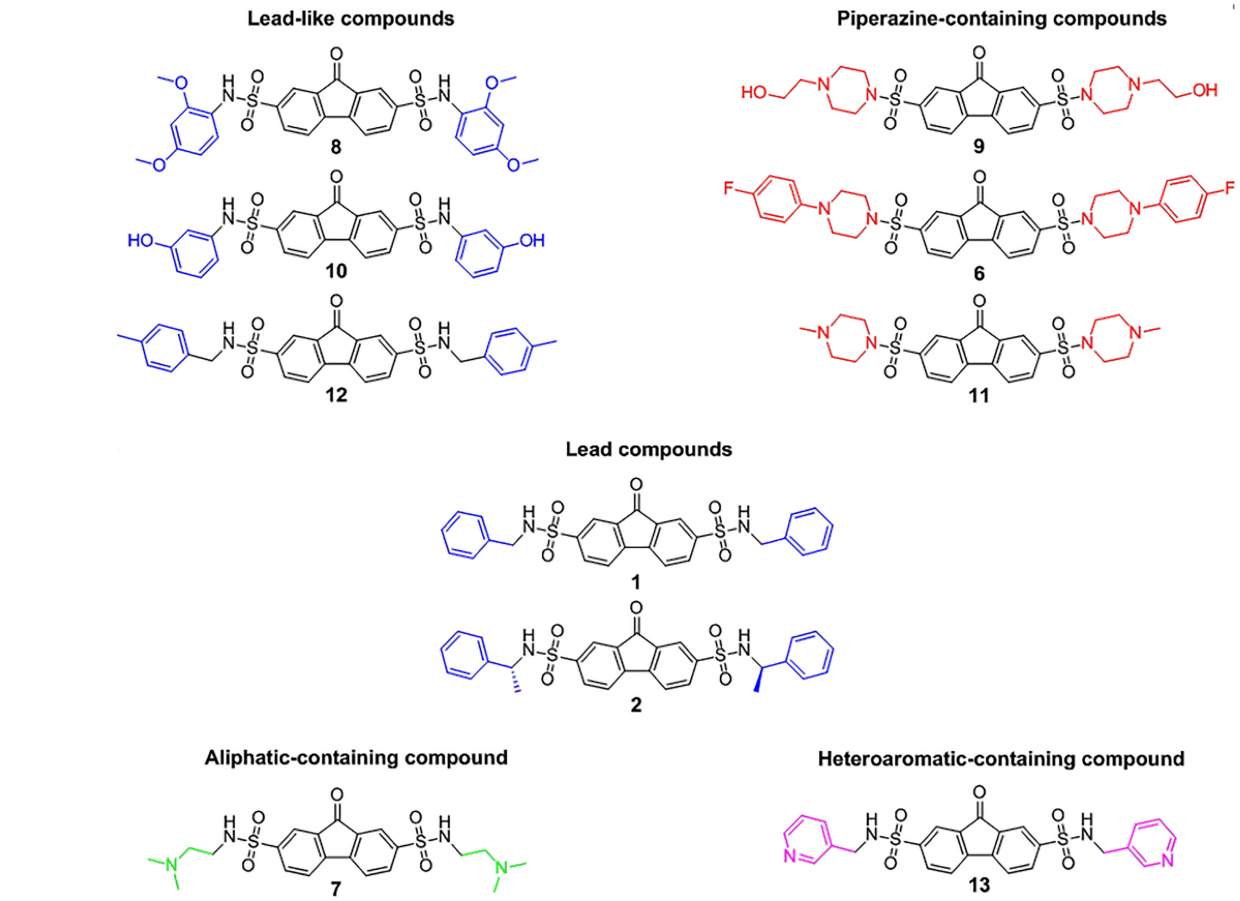

Figure 6. Selected compounds for synthesis, categorized into four groups.

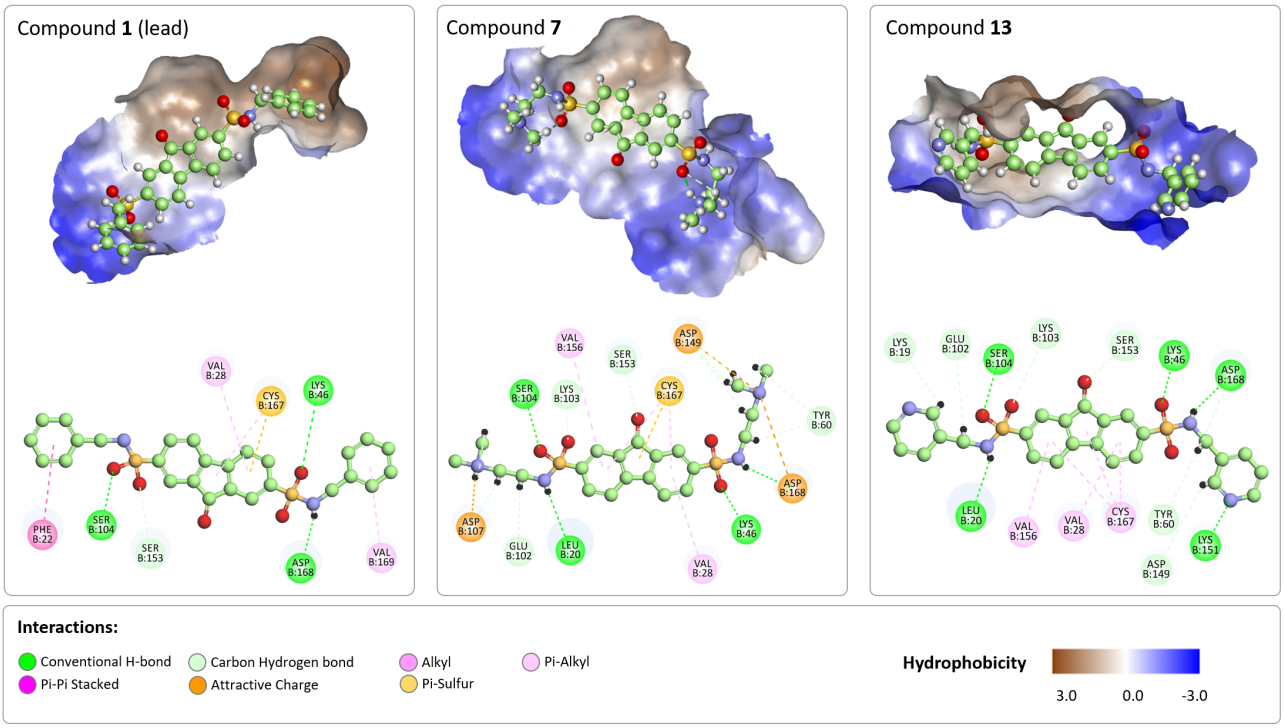

Figure 7. The binding modes of representative compounds **(7** and **13)** compared to that of the lead. Upper panel: 3D binding mode of the compounds. The binding site is shown as hydrophobic surface, and the docked compounds are in balls and sticks. Lower panel: The respective 2d interaction maps of the docked compounds with the active site's amino acids. Different types of interactions are colored differently.

ADME predictions of the selected compounds

To assess the ADME profile of the selected compounds, different physicochemical, pharmacokinetic parameters, druglikeness and medicinal chemistry friendliness were calculated using the SwissADME webserver (http://www.swissadme.ch/index.php) (Table 2). Establishing a preliminary ADME profile for lead compounds early in the drug discovery process is strongly advised to avoid dead ends. The predictions presented in Tables 2 revealed that the selected compounds have acceptable properties which make them good candidates for further optimization. Moreover, the medicinal chemistry friendliness predictions were encouraging where they showed no PAINS alerts and acceptable synthetic feasibility. Collectively, these predictions were promising to proceed in the synthesis of these compounds.

Table 2. Physicochemical, pharmacokinetics properties (ADME), drug-likeness, and medicinal chemistry friendliness for the selected compounds.

Index	Physicochemical descriptors						Pharmacokinetic (ADME)				Drug-likeness	Medicinal Chemistry	
No.	M. wt. (g/mol)	Rotatable bonds	No. of H-bonders	TPSA[a]	Lipophilicity log$P_{o/w}$	Water solubility	GI absorption	BBB permeant	P-gp[b] substrate	CYP inhibition[c]	Lipinski	PAINS[e]	Synthetic accessibility[f]
1	518.60	8	9	126.17	3.63	Poorly/ Moderately soluble	Low	No	No	1A2, 2C19, 2C9, 3A4	Yes	0	3.58
2	546.66	8	9	126.17	4.10	Poorly soluble	Low	No	No	2C9, 3A4	Yes	0	4.53
6	664.74	6	9	115.07	4.07	Poorly soluble	Low	No	No	2C9, 3A4	Yes	0	4.24
7	480.60	10	11	132.65	1.32	Soluble	High	No	Yes	2C9, 2C19, 3A4	Yes	0	3.70
8	610.65	10	11	163.09	3.56	Poorly/ Moderately soluble	Low	No	No	2C9, 2C19, 3A4	No	0	4.05
9	564.67	8	13	155.53	0.31	Soluble low	Low	No	Yes	2C9	No	0	4.06
10	522.55	6	11	166.63	2.68	Poorly/ Moderately soluble	Low	No	No	1A2, 2C19, 2C9, 3A4	Yes	0	3.43
11	502.65	4	7	108.59	3.41	Moderately soluble	High	No	Yes	2C9, 2C19, 3A4	Yes	0	3.69
12	546.66	8	9	126.17	4.37	Poorly soluble	Low	No	No	1A2, 2C19, 2C9, 3A4	Yes	0	3.80
13	520.58	8	11	151.95	2.17	Moderately soluble	Low	No	No	1A2, 2C19, 2C9, 3A4	Yes	0	3.46

a: Topological Polar Surface Area in Å^2.
b: Is it a P-glycoprotein substrate.
c: Inhibitor of which CYP450 enzyme.
d: Bioavailability: probability >10%.
e: Pan Assay Interference Structures.
f: Synthetic accessibility score: from 1 (very easy) to 10 (very difficult).

Synthesis

Chemistry

The top-scoring proposed analogs which were selected for synthesis were obtained following Figure 2. All analogs were synthesized from the common intermediate, 9-oxo-9H-fluorene-2,7-disulfonyl dichloride **5**, derived through electrophilic aromatic substitution of 9-fluorenone using chlorosulfonic acid. Subsequently intermediate compound **5** was reacted with the substituted amines to form the corresponding sulfonamide.

Initially, the chlorosulfonation of 9H-flourenone was attempted by stirring it with two equivalents of chlorosulfonic acid in a sealed flask at room temperature for 24 hours. The crude material was then used, without further purification to avoid decomposition of the reactive sulfonylchloride, to react with various alkyl amines. However, proton NMR indicated monochlorosulfonation of the aromatic ring.

Since no traces of the disulfonyl dichloride were detected, the reaction conditions, namely temperature, time and reagent equivalencies, were optimized to account for the decreased reactivity of the monochlorosulfonated fluorenone towards the second electrophilic aromatic substitution. The optimal conditions involved heating the aromatic ring with twelve equivalents of chlorosulfonic acid at temperatures ranging from 130 to 150°C for a duration of 5 days (24). Further attempts to enhance the yield of compound **5** by further elevating the temperature to 160 or 170°C led to the unfortunate outcome of product combustion.

General procedure for the synthesis of 9-oxo-9H-fluorene-2,7-disulfonyl Dichloride Intermediate 5

Chlorosulfonic acid (12 eq.) was added to 9-fluorenone and the resulting solution was refluxed at (130-150) °C for 5 days. The mixture was then allowed to cool to room temperature, and it was poured over ice, forming an insoluble yellow precipitate that was filtered and dried. The crude was used in the proceeding step without further purification.

*General procedure for the synthesis of Analogs (**1, 6 to 13**)*

Alkyl, aryl alkyl, or aryl amine (2eq.) was dissolved in anhydrous dichloromethane (1M) at 0°C under argon. Triethylamine (4eq.) and the disulfonyl dichloride **5** (1eq) were added at 0°C and then the mixture was stirred at room temperature for 24 h. The mixture was then washed with water and the organic layer was separated, dried over magnesium sulfate, filtered and evaporated under reduced pressure. The crude product was purified by Flash column chromatography using either ethyl acetate/ hexane or methanol/ dichloromethane. High-performance liquid chromatography (HPLC) was used to assess the purity of most of the synthesized compounds, which exceeded 95%.

N^2,N^7-Dibenzyl-9-oxo-9H-fluorene-2,7-disulfonamide (1)

Residue was purified by flash column chromatography with 0-100% ethyl acetate in hexane over 30 min to afford the title compound (0.053g, 13%) as a yellow powder. ^{1}H NMR (400 MHz, DMSO-d6): δ 8.37 (s, 2H, NH), 8.06 – 8.03 (m, 4H, H3, H4, H5 and H6), 7.87 (d, *J* = 4.4 Hz, 2H, H1 and H8), 7.20–7.14 (m, 10H, Ph-H), 4.05 (s, 4H, CH_2).^{13}C NMR (101 MHz, DMSO-d6): δ 190.2, 145.7 (2C), 143 (2C), 137.4 (2C), 134.4 (2C), 133.8 (2C), 128.4 (4C), 127.9 (4C), 127.3 (2C), 123.0 (2C), 122.1 (2C), 46.4 (2C). HRMS (ESI) m/z: Calculated for $C_{27}H_{21}N_2O_5S_2$ $[M-H]^-$: 517.0897, found 517.0899.

2,7-Bis((4-(4-fluorophenyl)piperazin-1-yl)sulfonyl)-9H-fluoren-9-one (6)

Residue was purified by flash column chromatography with 0-100% ethyl acetate in hexane over 30 min to afford the title compound (0.019g, 15%) as a yellow powder. ^{1}H NMR (400 MHz, DMSO-d6): δ 8.25 (d, *J* = 7.5 Hz, 2H, H4 and H5), 8.09 (d, *J* = 7.5 Hz, 2H, H3 and H6), 7.88 (s, H2, H1 and H8), 7.02-6.98 (m, 4H, H3', H3", H5' and H5"), 6.90-6.89 (m, 4H, H2', H2", H6'and H6"), 3.12 – 3.10 (m, 16H, pip-H). ^{13}C NMR (101 MHz, DMSO-d6): δ 190.4, 157.1 (d, *J* = 237.5 Hz, 2C, C-F), 147.8 (2C), 147.0 (2C), 137.5 (2C), 135.4 (2C), 135.2 (2C), 124.1 (2C), 123.2 (2C), 118.7 (d, *J* = 7.7 Hz, 4C), 116.0 (d, *J* = 22.1 Hz, 4C), 49.3 (4C), 46.4 (4C). HRMS (ESI) m/z: Calculated for $C_{33}H_{31}F_2N_4O_5S_2$ $[M+H]^+$: 665.1698, found 665.1711.

N^2,N^7-Bis(2-(dimethylamino)ethyl)-9-oxo-9H-fluorene-2,7-disulfonamide (7)

Residue was purified by flash column chromatography with 0-100% methanol in dichlormethane over 35 min to afford the title compound (0.094g, 21%) as an orange powder. ^{1}H NMR (400 MHz, DMSO-d6) δ: 8.24 (d, *J* = 8.2 Hz, 2H, H4 and H5), 8.18 (d, *J* = 8.2 Hz, 2H, H3 and H6), 8.06 (s, 2H, H1 and H8), 3.10 (t, *J* = 6.6 Hz, 4H, SO_2NCH_2), 2.83 (t, *J* = 6.6 Hz, 4H, NCH_2), 2.50 (s, 12H, NCH_3). ^{13}C NMR (101 MHz, DMSO-d6) δ: 190.0, 145.7 (2C), 142.0 (2C), 134.3 (2C), 133.8 (2C), 123.0 (2C), 121.9 (2C), 56.5 (2C), 43.2 (4C). HRMS (ESI) m/z: Calculated for $C_{21}H_{29}N_4O_5S_2$ $[M+H]^+$: 481.1573, found 481.1551.

N^2,N^7-Bis(2,4-dimethoxyphenyl)-9-oxo-9H-fluorene-2,7-disulfonamide (8)

Residue was purified by flash column chromatography with 0-50% ethylacetate in hexane over 45 min to afford the title compound (0.016g, 48%) as an orange powder. ^{1}H NMR (400 MHz, $CDCl_3$) δ: 8.05 (s, 2H, H1 and H8), 7.86 (d, *J* = 8.4 Hz, 2H, Ar-H), 7.57 (d, *J* = 8.8 Hz, 2H, Ar-H), 7.45 (d, *J* = 8.4 Hz, 2H, Ar-H), 6.75 (s, 2H, NH), 6.45 (dd, *J* = 8.8, 2.6 Hz, 2H, H5' and H5"), 6.26 (d, *J* = 2.6 Hz, 2H, H3' and H3"), 3.75 (s, 6H, CH_3), 3.53 (s, 6H, CH_3). ^{13}C NMR (101 MHz, DMSO-d6) δ: 189.9, 158.8 (2C), 154.3 (2C), 145.1 (2C), 142.4 (2C), 133.5 (2C), 133.4 (2C), 128.7 (2C), 122.0 (2C), 121.8 (2C), 116.7 (2C), 104.4 (2C), 98.6 (2C), 55.0 (2C), 54.8 (2C). HRMS (ESI) m/z: Calculated for $C_{29}H_{25}N_2O_9S_2$ $[M-H]^-$: 609.1007, found 609.1013.

2,7-Bis((4-(2-hydroxyethyl)piperazin-1-yl)sulfonyl)-9H-fluoren-9-one (9)

Residue was purified by flash column chromatography with 0-100% methanol in dichlormethane over 40 min to afford the title compound (0.044g, 40%) as an orange powder. ^{1}H NMR (400 MHz, $CDCl_3$) δ: 8.09 (s, 2H, H1 and H8), 8.00 (d, *J* = 7.8 Hz, 2H, H4 and H5), 7.82 (d, *J* = 7.8 Hz, 2H, H3 and H5), 3.59-3.57 (m, 4H, CH_2), 3.12 (m, 8H, CH_2), 2.63-2.61 (m, 8H, , CH_2), 2.57-2.54 (m, 4H, , CH_2). ^{13}C NMR (101 MHz, $CDCl_3$) δ: 190.1, 146.6 (2C), 138.5 (2C), 135.2 (2C), 134.8 (2C), 124.1 (2C), 122.1 (2C), 59.2 (2C), 58.0 (2C), 52.2 (4C), 46.3 (4C). HRMS (ESI) m/z: Calculated for $C_{25}H_{33}N_4O_7S_2$ $[M+H]^+$: 565.1785, found 565.1759.

N^2,N^7-Bis(3-hydroxyphenyl)-9-oxo-9H-fluorene-2,7-disulfonamide (10)

Residue was purified by flash column chromatography with 0-100% ethylacetate in hexane over 30 min to afford the title compound (0.016g, 44%) as an orange powder. ^{1}H NMR (400 MHz, DMSO-d6) δ: 8.31 (d, *J* = 7.9 Hz, 2H, H4 and H5), 8.21 (d, *J* = 7.9 Hz, 2H, H3 and H6), 7.96 (s, 2H, H1 and H8), 6.98-6.94 (m, 2H, H5' and H5"), 6.47 (d, *J* = 7.9 Hz, 2H, HO-Ph-H), 6.29 (s, 2H, H2' and H2"), 6.13 (d, 2H, *J* = 7.9 Hz, HO-Ph-H), 5.41 (s, OH). ^{13}C NMR (101 MHz, DMSO-d6) δ: 188.5, 150.2 (2C), 149.6 (2C), 146.8 (2C), 136.5 (2C), 135.1 (2C), 134.3 (2C), 129.7 (2C), 123.6 (2C), 122.7 (2C), 112.5 (2C), 107.7 (2C), 106.1 (2C). HRMS (ESI) m/z: Calculated for $C_{25}H_{19}N_2O_7S_2$ $[M+H]^+$: 523.0628, found 523.0605.

2,7-Bis((4-methylpiperazin-1-yl)sulfonyl)-9H-fluoren-9-one (11)

Residue was purified by flash column chromatography with 0-100% methanol in dichlormethane over 40 min to afford the title compound (0.1g, 38%) as a yellow powder. ^{1}H NMR (400 MHz, DMSO-d6) δ: 8.38 (d, *J* = 7.8 Hz, 2H, H4 and H5), 8.18 (d, , *J* = 7.8 Hz, 2H, H3 and H6), 7.98 (s, 2H, H1 and H8), 3.01 (s, 8H, Pip-CH_2), 2.49 (s, 8H, Pip-CH_2), 2.26 (s, 6H, NCH_3). ^{13}C NMR (101 MHz, DMSO-d6) δ: 189.7, 146.2 (2C), 137.2 (2C), 134.6 (2C), 134.4 (2C), 123.3 (2C), 122.4 (2C), 53.3 (4C), 45.6 (4C), 45.1 (2C). HRMS (ESI) m/z: Calculated for $C_{23}H_{29}N_4O_5S_2$ $[M+H]^+$: 505.1574, found 505.1548.

N^2,N^7-Bis(4-methylbenzyl)-9-oxo-9H-fluorene-2,7-disulfonamide (12)

Residue was purified by flash column chromatography with 0-100% ethylacetate in hexane over 40 min to afford the title compound (0.017g, 35%) as a yellow powder. ^{1}H NMR (400 MHz, DMSO-d6) δ: 8.33 (s, 2H, NH), 8.07 (d, *J* = 7.8 Hz, 4H, H4 and H5), 8.02 (d, *J* = 7.8 Hz, 4H, H3 and H6), 7.83 (s, 2H, H1 and H8), 7.06 (d, *J* = 7.8 Hz, 4H, H2', H6', H2" and H6"), 6.98 (d, *J* = 7.8 Hz, 4H, H3', H3", H5' and H5"), 4.00 (s, 4H, NCH_2), 2.13 (s, 6H, Ph-CH_3). ^{13}C NMR (101 MHz, DMSO-d6) δ: 190.1, 145.6 (2C), 143.0 (2C), 136.4 (2C), 134.3 (2C), 134.2 (2C), 133.8 (2C), 128.9 (4C), 127.9 (4C), 122.9 (2C), 122.0 (2C), 46.2 (2C), 20.7 (2C). HRMS (ESI) m/z: Calculated for $C_{29}H_{27}N_2O_5S_2$ $[M+H]^+$: 547.1356, found 547.1334.

9-Oxo-N^2,N^7-bis(pyridin-3-ylmethyl)-9H-fluorene-2,7-disulfonamide (13)

Residue was purified by flash column chromatography with 0-20% methanol in dichlormethane over 30 min to afford the title compound (0.021g, 43%) as a yellow powder. ^{1}H NMR (400 MHz, DMSO-d6) δ: 8.50 (d, 2H, NH), 8.42 (s, 2H, H2' and H2"), 8.39 (d, *J* = 3.8 Hz, 2H, Py-H), 8.13 (d, *J* = 7.9 Hz, 2H, H4 and H5), 8.07 (d, *J* = 7.9 Hz, 2H, H3 and H6), 7.92 (s, 2H, H1 and H8), 7.65 (d, *J* = 7.9 Hz, 2H, Py-H), 7.28 (dd, *J* = 7.9, 3.8 Hz, 2H, Py-H), 4.13 (s, 4H, NCH_2). ^{13}C NMR (101 MHz, DMSO-d6) δ: 189.8, 148.9 (2C), 148.3 (2C), 145.4 (2C), 142.5 (2C), 135.3 (2C), 134.1 (2C), 133.6 (2C), 132.8 (2C), 123.2 (2C), 122.8 (2C), 121.8 (2C), 43.6 (2C). HRMS (ESI) m/z: Calculated for $C_{25}H_{21}N_4O_5S_2$ $[M+H]^+$: 521.0948, found 521.0932.

Biological Evaluation

The nine synthesized compounds were biologically tested to evaluate their inhibitory activities against the TOPK enzyme. The *in vitro* assay was performed by Reaction Biology Corp. (Malvern, PA, USA). The results are shown in Table 2 with the average IC_{50}. Figure 8 depicts the dose-response curves of compound **13** as compared to staurosporine (IC_{50} = 17 nM).

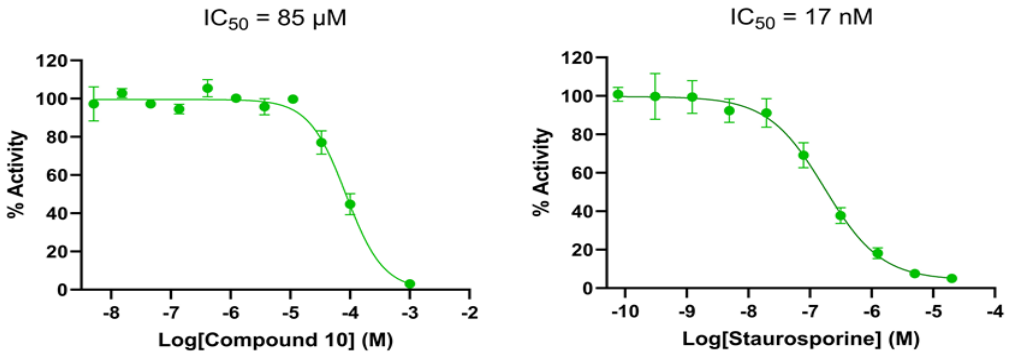

Figure 8. The dose-response curves of compound **13** and the positive control (staurosporine).

The *in vitro* assay analysis revealed some key insights into the structure-activity relationship of these TOPK inhibitors. Substituents on the benzene ring of the benzylamine moiety (compounds **8**, **10**, and **12**) resulted in a complete loss of activity. Similarly, replacing the benzylamine group with piperazine-containing moieties (compounds **6**, **9**, and **11**) or an aliphatic moiety (compound **7**) also abolished inhibitory effects.

However, a promising finding emerged. Isosteric replacement of the benzene ring with a pyridine ring in compound **13** yielded moderate activity (IC_{50} = 86 μM) compared to the lead compound *1* (IC_{50} = 54 μM). While the number of analogs tested is still limited, these results suggest that the presence of a hydrophobic moiety might be crucial for binding to the TOPK enzyme's active site. This hypothesis aligns with the observation that bulky substituents (compounds **6**, **8**, and **12**) and increased polarity (compounds **7**, **9**, **10**, and **11**) generally led to inactivity. The slightly lower activity of compound **13** compared to compound **1** might be due to the pyridine ring's slightly higher polarity compared to benzene.

Further investigation with a larger and more diverse set of analogs is warranted to solidify these initial findings and optimize the design of potent TOPK inhibitors.

Conclusion

TOPK plays a critical role in cancer by promoting proliferation, metastasis, and impacting prognosis. Inhibiting TOPK offers a potential avenue for cancer treatment with reduced side effects due to its limited expression in normal cells.

Building on our prior discovery of TOPK inhibitors through computational modeling, 92 analogs were designed based on a promising lead compound. These analogs were docked into the TOPK homology model's ATP binding site, and the resulting poses were analyzed for binding energy and visually inspected. Nine compounds (including the lead) were then synthesized and tested for TOPK inhibitory activity in vitro. While only compound **13** showed moderate activity (IC_{50} = 86 μM) compared to the lead (compound **1**, IC_{50} = 54 μM), these results provide valuable insights for future inhibitor design.

Biological evaluation revealed a clear structure-activity relationship (SAR) for the N-substituents. Modifications with bulky groups (substituted benzylamine, piperazine, or aliphatic moieties) abolished activity. However, replacing the benzene ring with a pyridine (compound **13**) maintained moderate inhibition, suggesting a potential path for future design. Further analog exploration is necessary to refine the SAR and identify optimal TOPK inhibitors.

Acknowledgments

This work was funded by the Deanship of Scientific Research at Jordan University of Science and Technology.

Author Contributions

Manar Al-Sarhan: Investigation. Lara I. Fakhouri: Conceptualization, Methodology, Project Administration, Supervision, Writing - Review & Editing. Nizar A. Al-Shar': Conceptualization, Methodology, Project Administration, Funding Acquisition, Visualization, Supervision, Writing - Original Draft. Tamam El-Elimat: Investigation. Aref Zayed: Investigation

Conflict of Interest

The authors declare that they have no conflict of interest.

Supplementary Data

Supplementary data are available at https://doi.org/10.34172/PS.2024.20.

References

1. Understanding c ancer. https://www.cancer.gov/about-cancer/understanding. Accessed on June 2023.
2. The genetics of cancer. https://www.cancer.gov/about-cancer/causes-prevention/genetics. Accessed on June 2023.
3. Sung H, Ferlay J, Siegel RL, Laversanne M, Soerjomataram I, Jemal A, et al. Global cancer statistics 2020: globocan estimates of incidence and mortality worldwide for 36 cancers in 185 countries. CA Cancer J Clin. 2021;71(3):209-49. doi:10.3322/caac.21660.
4. Rueff J, Rodrigues AS. Cancer drug resistance: a brief overview from a genetic viewpoint. Methods Mol Biol. 2016;1395:1-18.10.1007/978-1-4939-3347-1_1
5. Padma VV. An overview of targeted cancer therapy. Biomedicine. 2015;5(4):19. doi:10.7603/s40681-015-0019-4.
6. Zhong L, Li Y, Xiong L, Wang W, Wu M, Yuan T, et al. Small molecules in targeted cancer therapy: advances, challenges, and future perspectives. Signal Transduct Target Ther. 2021;6(1):201. doi:10.1038/s41392-021-00572-w.
7. Cohen P, Alessi DR. Kinase drug discovery – what's next in the field? ACS Chemical Biology. 2013;8(1):96-104. doi:10.1021/cb300610s
8. Cohen P, Cross D, Jänne PA. Kinase drug discovery 20 years after imatinib: progress and future directions. Nat Rev Drug Discov. 2021;20(7):551-69. doi:10.1038/s41573-021-00195-4
9. Hernandez-Boluda JC, Cervantes F. Imatinib mesylate (Gleevec, Glivec): a new therapy for chronic myeloid leukemia and other malignancies. Drugs Today (Barc). 2002;38(9):601-13. doi:10.1358/dot.2002.38.9.696536
10. Abe Y, Matsumoto S, Kito K, Ueda N. Cloning and expression of a novel MAPKK-like protein kinase, lymphokine-activated killer T-cell-originated protein kinase, specifically expressed in the testis and activated lymphoid cells. J Biol Chem. 2000;275(28):21525-31. doi:10.1074/jbc.M909629199

11. Huang H, Lee MH, Liu K, Dong Z, Ryoo Z, Kim MO. PBK/TOPK: An Effective Drug Target with Diverse Therapeutic Potential. Cancers (Basel). 2021;13(9):2232. doi:10.3390/cancers13092232
12. Park JH, Nishidate T, Nakamura Y, Katagiri T. Critical roles of T-LAK cell-originated protein kinase in cytokinesis. Cancer Sci. 2010;101(2):403-11. doi:10.1111/j.1349-7006.2009.01400.x
13. Han Z, Li L, Huang Y, Zhao H, Luo Y. PBK/TOPK: a therapeutic target worthy of attention. Cells. 2021;10(2):371. doi:10.3390/cells10020371
14. Fujibuchi T, Abe Y, Takeuchi T, Ueda N, Shigemoto K, Yamamoto H, et al. Expression and phosphorylation of TOPK during spermatogenesis. Dev Growth Differ. 2005;47(9):637-44. doi:10.1111/j.1440-169X.2005.00834.x
15. Simons-Evelyn M, Bailey-Dell K, Toretsky JA, Ross DD, Fenton R, Kalvakolanu D, et al. PBK/TOPK is a novel mitotic kinase which is upregulated in Burkitt's lymphoma and other highly proliferative malignant cells. Blood Cells Mol Dis. 2001;27(5):825-9. doi:10.1006/bcmd.2001.0452
16. Dong C, Tang X, Xie Y, Zou Q, Yang X, Zhou H. The crystal structure of an inactive dimer of PDZ-binding kinase. Biochem Biophys Res Commun. 2016;476(4):586-93. doi:10.1016/j.bbrc.2016.05.166
17. Fakhouri LI, Al-Shar'i NA. The design of TOPK inhibitors using structure-based pharmacophore modeling and molecular docking based on an MD-refined homology model. Mol Divers. 2022;26(5):2679-702. doi:10.1007/s11030-021-10361-w
18. Discovery Studio. version 2020 ed. San Diego, CA, USA: Accelrys Inc.; 2020.
19. Wu G, Robertson DH, Brooks CL 3rd, Vieth M. Detailed analysis of grid-based molecular docking: A case study of CDOCKER-A CHARMm-based MD docking algorithm. J Comput Chem. 2003;24(13):1549-62. doi:10.1002/jcc.10306
20. Wang J, Li F, Pei W, Yang M, Wu Y, Ma D, et al. Selective cleavage of the N-propargyl group from sulfonamides and amides under ruthenium catalysis. Tetrahedron Lett. 2018;59(20):1902-5. doi:10.1016/j.tetlet.2018.03.046
21. Anastassiadis T, Deacon SW, Devarajan K, Ma H, Peterson JR. Comprehensive assay of kinase catalytic activity reveals features of kinase inhibitor selectivity. Nat Biotechnol. 2011;29(11):1039-45. doi:10.1038/nbt.2017.
22. Kim DJ, Li Y, Reddy K, Lee MH, Kim MO, Cho YY, et al. Novel TOPK inhibitor HI-TOPK-032 effectively suppresses colon cancer growth. Cancer Res. 2012;72(12):3060-8. doi:10.1158/0008-5472.Can-11-3851
23. Wang MY, Lin ZR, Cao Y, Zheng LS, Peng LX, Sun R, et al. PDZ binding kinase (PBK) is a theranostic target for nasopharyngeal carcinoma: driving tumor growth via ROS signaling and correlating with patient survival. Oncotarget. 2016;7(18):26604-16. doi:10.18632/oncotarget.8445
24. Ishikawa C, Senba M, Mori N. Mitotic kinase PBK/TOPK as a therapeutic target for adult T-cell leukemia/lymphoma. Int J Oncol. 2018;53(2):801-14. doi:10.3892/ijo.2018.4427
25. Matsuo Y, Park JH, Miyamoto T, Yamamoto S, Hisada S, Alachkar H, Nakamura Y. TOPK inhibitor induces complete tumor regression in xenograft models of human cancer through inhibition of cytokinesis. Sci Transl Med. 2014;6(259):259ra145. doi:10.1126/scitranslmed.3010277
26. Nakamura Y, Matsuo Y, Hisada S, Ahmed F, Huntley R, Sajjadi-Hashemi Z, et al. Tricyclic compounds and PBK inhibitors containing the same. European Patent EP2552206B1 ; 2016.
27. Zhu Y, Alqahtani S, Hu X. Aromatic rings as molecular determinants for the molecular recognition of protein kinase inhibitors. Molecules. 2021;26(6):1776. doi:10.3390/molecules26061776.28
28. Perry PJ, Read MA, Davies RT, Gowan SM, Reszka AP, Wood AA, Kelland LR, Neidle S. 2,7-Disubstituted amidofluorenone derivatives as inhibitors of human telomerase. J Med Chem. 1999;42(14):2679-84. doi:10.1021/jm990084q
29. Lee S, Esteva-Font C, Phuan PW, Anderson MO, Verkman AS. Discovery, synthesis and structure-activity analysis of symmetrical 2,7-disubstituted fluorenones as urea transporter inhibitors. Medchemcomm. 2015;6:1278-1284. doi:10.1039/C5MD00198F
30. Kitchen DB, Decornez H, Furr JR, Bajorath J. Docking and scoring in virtual screening for drug discovery: methods and applications. Nat Rev Drug Discov. 2004;3(11):935-49. doi:10.1038/nrd1549
31. Kleinjung J, Fraternali F. Design and application of implicit solvent models in biomolecular simulations. Curr Opin Struct Biol. 2014;25(100):126-34. doi:10.1016/j.sbi.2014.04.003
32. Genheden S, Ryde U. The MM/PBSA and MM/GBSA methods to estimate ligand-binding affinities. Expert Opin Drug Discov. 2015;10(5):449-61. doi:10.1517/17460441.2015.1032936